View metadata, citation and similar papers at core.ac.uk

brought to you by CORE

provided by The University of Utah: J. Willard Marriott Digital Library

PHYSICAL REVIEW B **79**, 195202 (2009)

Direct evidence of electron spin polarization from an organic-based magnet: $[Fe^{II}(TCNE)(NCMe)_2][Fe^{III}Cl_4]$

A. N. Caruso,[1,*] Konstantin I. Pokhodnya,[2,3,4] William W. Shum,[2] W. Y. Ching,[1] Bridger Anderson,[3] M. T. Bremer,[3] E. Vescovo,[5] Paul Rulis,[1] A. J. Epstein,[4] and Joel S. Miller[2]

[1]*Department of Physics, University of Missouri–Kansas City, Kansas City, Missouri 64110, USA*

[2]*Department of Chemistry, University of Utah, Salt Lake City, Utah 84112-0850, USA*

[3]*Center for Nanoscale Science and Engineering, North Dakota State University, Fargo, North Dakota 58102, USA*

[4]*Department of Physics and Department of Chemistry, The Ohio State University, Columbus, Ohio 43210-1117, USA*

[5]*National Synchrotron Light Source, Brookhaven National Laboratory, Upton, New York 11973, USA*

(Received 26 March 2009; published 4 May 2009)

Direct evidence of an organic-based magnet with a finite electron spin polarization at the Fermi edge is shown from spin-resolved photoemission of the $[Fe^{II}(TCNE)(NCMe)_2][Fe^{III}Cl_4]$ organic-based magnet. The 23% majority-based spin polarization at the Fermi edge is observed at 80 K in zero applied field. *Ab initio* calculations at the density functional level (0 K) are in accord with a semiconductor with 100% majority-based electron spin polarization at the band edges, commensurate with our experimental results and model prediction for a half-semiconductor. Organic-based magnets may prove to be important for realizing polarized electron injection into semiconductors for magnetoelectronic applications.

DOI: 10.1103/PhysRevB.79.195202 PACS number(s): 75.25.+z, 71.15.Mb, 71.20.Rv, 75.30.Et

I. INTRODUCTION

Organic-based magnets present a new class of materials with capabilities toward magnetoelectronic applications not possible from inorganic magnets. For example, organic-based solids offer high interfacial stability because of small differences between their surface and bulk free energies, long spin carrier lifetimes due to low spin-orbit and/or hyperfine interactions, and flexible tuning of the valence and conduction band edges.[1–3] Further, some organic-based magnets may offer very high electron spin polarization, akin to a half-metal, but this idea has only been indirectly demonstrated.[4,5] We show here direct evidence of an organic-based magnet exhibiting electron spin polarization in the valence band, specifically, 23% polarization at the Fermi edge from spin-resolved photoemission of the $[Fe^{II}(TCNE)(NCMe)_2][Fe^{III}Cl_4]$ organic-based magnet.[6] *Ab initio* calculations (0 K) reveal a half-semiconductor, with 100% majority-based electron spin polarization at the band edges. Most importantly, organic-based magnets may enable semiconductor magnetoelectronics,[7] where inorganic solids have struggled[8] because of their demonstrated ability to simultaneously exhibit a semiconductor character and finite spin polarization of carriers at room temperature.[9]

A family of organic-based magnets of $M^{II}[TCNE]_x \cdot zS$ (M=V, Mn, Fe, Co, and Ni; TCNE=tetracyanoethylene; and S=CH_2Cl_2) composition exhibits ordering temperatures, T_c, ranging from 44 (M=Co, Ni) (Ref. 10) to ~400 K for M=V.[11] The latter is also available as solvent-free thin films.[12,13] Although the detailed magnetic structures for the $M^{II}[TCNE]_x \cdot zS$ (M=V, Mn, Fe, Co, and Ni) compounds have yet to be established, magnetic ordering is proposed to occur via strong antiferromagnetic (AFM) exchange between the transition metal 3d and $[TCNE]^{\bullet-}$ π^* anion-radical unpaired spins.[13–15] The spin polarized electronic structure [Fig. 1(a)] for the most extensively studied member of this family of compounds, $V^{II}[TCNE]_x \cdot zS$ was proposed to principally arise from the on-site Coulomb repulsion within the $[TCNE]^{\bullet-}$ π^* individually and AFM coupling between the V^{II} 3d and $[TCNE]^{\bullet-}$ π^* unpaired spins.[4,5] As a consequence of the strong AFM exchange between the unpaired V^{II} 3d electron spins and the $[TCNE]^{\bullet-}$ π^* unpaired spins,[4,5] the Coulomb energy (U_C) split $[TCNE]^{\bullet-}$ π^* Hubbard subbands[16] each exhibit a single polarization or single spin filling. The result is a half-semiconductor, similar to a half-metal, where the valence and conduction band edges are both 100% majority polarized. As the spin polarized upper $[TCNE]^{\bullet-}$ π^* subband is likely the lowest unoccupied state, it is reasonable to assume that the charge carriers excited over the gap—into the conduction band—are majority spin polarized.

Recent magnetoresistance studies of $V[TCNE]_x$ films have inferred a spin-driven effect attributed to a spin polarized density of states (DOS).[4,5,18] Magnetic circular dichroism of the V $L_{2,3}$ edge and resonant photoemission at the Fermi edge of $V[TCNE]_x$ and $Rb^+[TCNE]^{\bullet-}$ support the presence of nonoverlapping spin polarized bands and the potential for very high spin polarization close to E_F.[19–21] Magnetic circular dichroism of C and N in $V[TCNE]_x$ showed that the spin in the $V^{II}[TCNE]^{\bullet-}$ π^* orbital is delocalized across the $[TCNE]^{\bullet-}$ and is opposite in polarization to the spin on V^{II}.[21] However, magnetoresistance (MR) and spin-integrated photoelectron spectroscopy (PES) techniques are indirect means of observing a finite spin polarization. A direct means of determining binding energy-dependent electron spin polarization is from angle resolved spin polarized photoemission spectroscopy (SPPES),[22] as presented here.

The organic-based $[Fe^{II}(TCNE)(NCMe)_2][Fe^{III}Cl_4]$, **1**, ($T_c$=90 K) magnet was selected for initial SPPES because of its known crystalline structure[6] [Fig. 1(b)], modest air sensitivity, and strong potential for high electron spin polarization in the valence band. This structure is comprised of buckled monocationic $\{Fe^{II}-\mu_4-[TCNE]^{\bullet-}\}^+$ layers that are separated through space by the axially bound MeCN ligands.

 ©2009 The American Physical Society

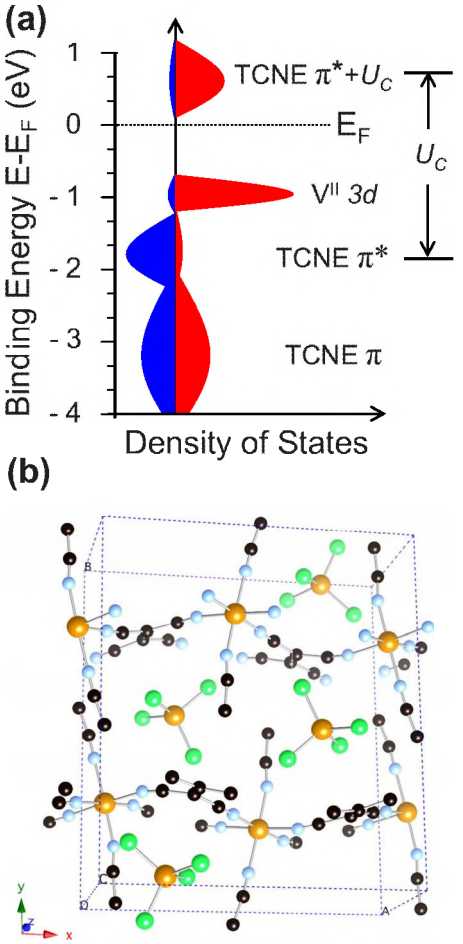

FIG. 1. (Color online) Electronic and crystal structure models of $V^{II}[TCNE]_x \cdot zS$ and **1**. (a) Schematic illustration of the effects of Coulomb repulsion, AFM coupling, and Pauli exclusion within and between the V^{II} 3*d* and $[TCNE]^{\bullet -}$ π^* in $V^{II}[TCNE]_x \cdot zS$ (modified from Refs. 4 and 5). The π^* splitting, caused by the large U_C (~2 eV), but modest transfer integral t (~0.1 eV), forms occupied lower (π^*) and unoccupied upper (π^*+U_C) subbands in accord with the Hubbard model (Ref. 16). Due to a strong AFM interaction between the $[TCNE]^{\bullet -}$ π^* and V^{II} 3*d* spins sites, the $[TCNE]^{\bullet -}$ electrons in the lower subband are spin polarized antiparallel to the V^{II} 3*d*. However, Pauli exclusion requires the spin polarization of the upper empty subband π^*+U_C to be antiparallel to the π^* or parallel to the V^{II} 3*d*. The implication of this model is a semiconductor with 100% polarization at the band edges, termed *half-semiconductor* (Refs. 4 and 5), following from *half-metal* where a solid is metallic in one spin direction and insulating in the other (Ref. 17). (b) Structure of **1** (Ref. 6) with Cl (green), C (black), N (blue), H (white), and Fe (yellow).

This results in an axially distorted octahedral coordination environment around each Fe^{II} ion. Further, the spin polarized electronic structure model for **1** may be generalized within the half-semiconductor model despite different TCNE stoichiometry and 3*d* (e_g and t_{2g}) filling; it is for this reason that we draw a parallel between previous indirect measurements for M=V, $x \sim 2$ vs M=Fe, $x \sim 2$ vs SPPES of M=Fe, x=1 here. The experimentally determined spin polarized electronic structure of **1** is complimented by calculations using *ab initio* methods.[23]

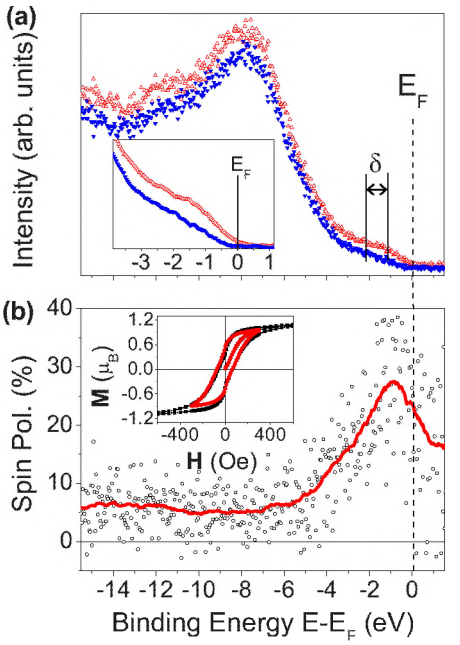

FIG. 2. (Color online) SPPES and polarization of 1. (a) Spin majority (△) and spin minority (▼) electron dispersion curves of **1** completed at 80 K with a photon energy of 47.5 eV and photoelectrons collected at surface normal. Inset: log (intensity) to illustrate the difference in majority/minority states near the Fermi edge demonstrating 23% majority polarization at the Fermi edge. (b) Electron spin polarization computed from the raw spectra. The solid line (−) is an averaging guide. Inset: 80 K $M(h)$, using a 2 T saturation field (■) and minor loop 300 Oe field (●).

II. EXPERIMENTAL AND CALCULATION DETAILS

1 was synthesized as described previously.[6] The polycrystalline sample was pressed into a 7-mm-diameter × 0.5-mm-thick pellet at 0.5 kbar in a Dry-box and then loaded and transferred in <1 ppm O_2 and H_2O to a 10^{-8} Torr load lock and then a 5×10^{-11} Torr UHV chamber for photoemission, where the sample was immediately cooled to prevent solvent (MeCN) loss. The spin polarized photoemission was collected at the National Synchrotron Light Source, Beamline U5UA, utilizing an undulator with spherical grating monochromator and spin detection system.[24] The magnetization direction was flipped for each of the spectra collected by a pulsed 300 Oe field. When the 300 Oe pulsing field is applied—to switch the magnetization during the measurement—the minor loop (±0.03 T) overlaps within 3% of the major loop (±1.0 T), indicating that the spectra collected represent the true polarization at remanence at 80 K, despite applying less than the field required for saturation [Fig. 2(b)]. All spectra shown were obtained at 80 K with the incident vector potential **A** at 45° with respect to surface normal and the photoelectrons collected along $k_{\|}$=0 or surface normal and incident photon energy of $h\nu$=47.5 eV. The polarization was determined by

$$P = \frac{1}{S}\frac{\sqrt{I_L^+ I_R^-} - \sqrt{I_L^- I_R^+}}{\sqrt{I_L^- I_R^-} + \sqrt{I_L^+ I_R^+}} \propto \frac{D_\uparrow(E) - D_\downarrow(E)}{D_\uparrow(E) + D_\downarrow(E)}, \quad (1)$$

where P is the polarization, S is the Sherman function of the analyzer [taken as 0.15 (Ref. 24)], I is the intensity, L/R are

the left/right channeltrons, and +/− is the magnetization direction during collection; $D(E)$ are the majority (↑) and minority (↓) DOSs. Note that the photoemission spectra shown were repeatable over multiple positions of the pressed pellet and that the background polarization from the surface sensitive SPPES is important as it demonstrates that **1** was transferred successfully without oxygen-induced decomposition. Further, it should be noted that **1** decomposes from the high intensity available from the multipole wiggler (10^{14} photons/cm^2/s) within 13 h, wherein the polarization also goes to zero and is in accord with **1** being ferrimagnetic.[6] Lastly, the Fermi level and spin-polarization asymmetry were calibrated by Au(111), wherein the asymmetry was determined at ±1.2%.

The spin polarized electronic structure was calculated using the first-principles orthogonalized linear combination of atomic orbital (OLCAO) method. OLCAO is a density-functional-theory-based local orbital method employing the local density approximation (LDA). This method is particularly suitable for complex low symmetry crystals such as **1**.[23] The calculation used a full basis set expansion consisting of atomic orbitals of Fe ([Ar] core plus $3d$,$4s$,$4p$,$5s$,$5p$,$4d$), N ($1s$,$2s$,$2p$,$3s$,$3p$), C ($1s$,$2s$,$2p$,$3s$,$3p$), and H ($1s$,$2s$,$2p$). To achieve high accuracy, 60 k points in the irreducible portion of the Brillouin zone of the orthorhombic cell were used with the total energy convergence of 0.0001 eV/cell. Additional tests using 90 k points show no discernable difference.

III. RESULTS AND DISCUSSION

SPPES yields a quantity proportional to the spin-resolved DOS as a function of binding energy. The spectra shown in Fig. 2(a) demonstrate a strong (~6%) background polarization and significant difference in the intensity and binding energy position of the spin-resolved bands. The intensity and exchange differences of the spin-resolved photoemission features in Fig. 2(a) yield the polarization (P) in Fig. 2(b) where P is the ratio of the difference to the sum of spin-up and spin-down photoemission intensities.[22]

The SPPES of Fig. 2(a) shows peaks of opposite spin polarization with a splitting (labeled δ) of 0.9 eV between −1.2 and −2.1 eV and a much less pronounced 0.5 eV splitting between −11.9 and −11.4 eV. No splitting is observed for the broad feature centered at −7 eV, as expected for doubly occupied predominantly carbon and nitrogen $2p$ π (sigma) related orbitals. From previous resonant photoemission of V[TCNE]$_x$,[19] the [TCNE]$^{\bullet-}$ π^* and V $3d$ states were found at −2.5 and −1 eV, respectively. Because a lower binding energy is expected for the highest occupied vanadium states relative to the highest occupied iron states, i.e., the V^{II} t_{2g} vs Fe^{II} e_g, from comparison VO and FeO photoemission,[25,26] and from recent[27] resonant photoemission of Fe[TCNE]$_x$, for $x \sim 2$, a greater overlap in binding energy between the Fe^{II} $3d$ (t_{2g},e_g) and [TCNE]$^{\bullet-}$ π^* bands of **1** may occur. The shift toward higher binding energy of the Fe^{II} $3d$ highest occupied state should remove electron density from the Fermi edge causing a more insulating state. Further, the increased overlap between the Fe^{II} $3d$ and opposite spin [TCNE]$^{\bullet-}$ π^* may result in a reduced net spin polarization, relative to V[TCNE]$_x$. Indeed, a weak photoemission intensity and 23% remanent polarization are observed at E_F (Fig. 2). This observation supports that **1** is an organic-based magnet capable of spin injection. Three reasons are suggested for the origin of the measured 23% electron spin polarization relative to the predicted 100% following from the V^{II}[TCNE]$_x$•zS model.[4,5] First, the spectra were collected from a polycrystalline pellet [with two-dimensional (2D) Ising anisotropy], such that the ratio of remanent to saturation magnetizations (reduced magnetization) is less than unity (not a square loop), the photoemission is averaged over many crystallites, and the wave-vector-dependent resolution is lost. Second, the binding energy overlap and opposite polarization (AFM pairing) of the high spin Fe^{II} $3d$ and [TCNE]$^{\bullet-}$ π^* bands should cause energy-dependent partial polarization compensation. Lastly, since the spectra were collected at 80 K (=0.89 T_c) additional reduction in the polarization should arise from spin mixing due to phonon coupling.[28] If sufficiently large single crystals with single domains were available and the sample was cooled further, the 23% would very likely rectify within high-polarization (>90%) model. In lieu of such ideal experimental conditions, insight into the above assumptions is provided through the results of *ab initio* methods. The calculated results include the spin polarized band mapping and partial density of states (PDOS) breakdown of **1** without phonon interactions (zero kelvin calculation).

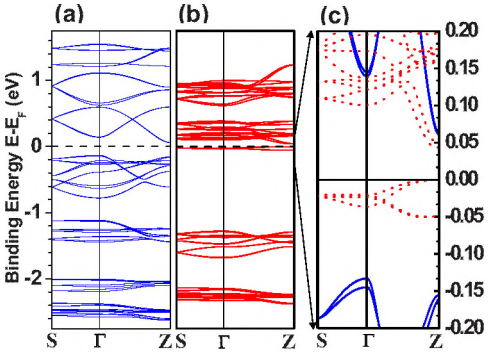

FIG. 3. (Color online) Calculated spin polarized band structure for the (a) spin minority and (b) spin majority bands. (c) Zoom in near the Fermi edge along two high symmetry directions where the dashed line (- - -) is spin majority and solid (−) spin minority.

A calculated band structure based on the crystal structure parameters of **1** (Ref. 6) using the OLCAO method[23] is shown in Figs. 3(a) and 3(b). Note that a significant dispersion difference (>500 vs <200 meV) exists for the minority [Fig. 3(a)] vs majority [Fig. 3(b)] occupied and unoccupied bands. This dispersion difference is likely due to the overlap of the Fe^{II} t_{2g} (d_{xz},d_{yz}) and [TCNE]$^{\bullet-}$ π^* minority states. The increased dispersion of the minority bands reflects the delocalization of the [TCNE]$^{\bullet-}$ π^* electrons in the solid's valence and conduction bands and the antiferromagnetic exchange between Fe^{II} t_{2g} and [TCNE]$^{\bullet-}$ π^*. In contrast, the majority spin band dispersion is very narrow which reflects that the majority spin levels reside principally on the Fe^{II}. Most importantly, a 40 meV gap [Fig. 3(c)] is calculated and con-

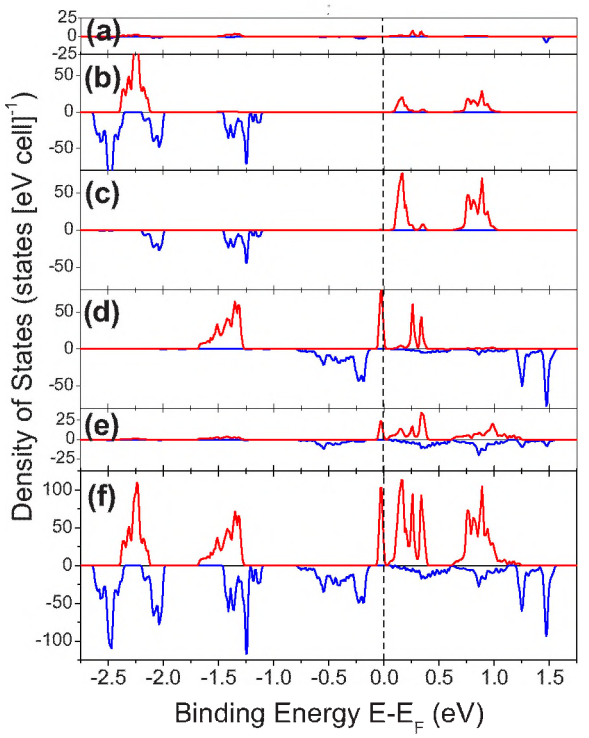

FIG. 4. (Color online) Calculated partial and total DOS as a function of binding energy referenced to the E_F of **1** where each upper/lower panel is the respective spin majority/minority DOS: (a) MeCN, (b) Cl, (c) Fe^{III}, (d) Fe^{II}, and (e) TCNE. (f) denotes the total DOS.

strained by majority-only bands at the Z point, consistent with the half-semiconductor prediction for the $V^{II}[TCNE]_x \cdot zS$ family[4,5] and related high-polarization organic radical based systems.[29–31] When thermal broadening is taken into consideration, the results of the calculations reconcile with experiment regarding a finite DOS at E_F, where the inset in Fig. 2(a) shows the intensity of the position of the highest occupied state. However, only 23% polarization is observed experimentally in this near Fermi region relative to the 100% calculated polarization. Though angle resolved, the lack of wave-vector conservation (k integrated) from the polycrystalline pellet does not allow for probe of individual Brillouin-zone points.

To further explore the spin-resolved photoemission, the spin-resolved partial PDOSs were calculated (Fig. 4). The PDOS (Fig. 4) shows the contributions from MeCN, Cl^-, Fe^{III}, Fe^{II}, and $[TCNE]^{\bullet -}$. The PDOSs were determined by the Mulliken scheme, and as such the relative intensities with regard to projected charge and magnetic moment should be taken only as qualitative. Further, because the interpretation of magnetic experiments suggests strong spin coupling[6] and on-site Coulomb repulsion[4–6,19,20] a more rigorous interpretation must also take into account the spin-dependent correlation effects arising from the electron-electron and other interactions from all constituents.

The calculated PDOSs for the Fe^{II} and $[TCNE]^{\bullet -}$ show strong energy space overlap for their occupied DOS, while the Fe^{III} and $[TCNE]^{\bullet -}$ reveal only moderate binding energy overlap for their unoccupied DOS, specifically, for those states centered at +0.15 and +0.85 eV. From a through-space exchange pathway perspective, the shortest distance between Cl from $[Fe^{III}Cl_4]^-$ and C or H from MeCN is 3.45 and 2.97 Å, respectively; both of which exceed the sum of their van der Waals radii. Therefore, an exchange interaction via Fe^{III} can only occur via a dipole-dipole interaction that is expected to be small; Mössbauer measurements down to 2 K and Brillouin fittings, however, provide no evidence that the Fe^{III} contributes to long-range magnetic ordering. Interestingly, the PDOSs show that the MeCN also has a strong binding energy and axial overlap with Fe^{II}. However, the lack of real-space overlap between the adjacent layers from MeCN to MeCN implies that **1** is a dominant 2D structural network consistent with its magnetic ground state.[6]

Although both experiment and calculation suggest that the highest occupied state of **1** is majority polarized, it is not clear, at finite temperature, whether the lowest unoccupied state will also be majority spin polarized. The *ab initio* results (0 K) of **1** here suggest that the lowest unoccupied state is majority spin polarized; however, the closest minority band is <25 meV away. An experimental determination of the spin polarization of this lowest unoccupied state is not straightforward[19,21] but is important, especially relative to those experimentally unrealized semiconductor-based magnetoelectronic applications.[7,9]

IV. SUMMARY

Spin-polarized ultraviolet photoemission of a pressed pellet of $[Fe^{II}(TCNE)(NCMe)_2][Fe^{III}Cl_4]$ revealed 23% polarization at the Fermi edge. *Ab initio* band-structure calculations suggest a 40 meV gap, and a 100% polarization at the valence, and conduction band edges at 0 K, in accord with a half-semiconductor. Finally, the observed electron spin polarization suggests that organic-based magnets should be capable electron spin injectors for magnetoelectronic applications.

ACKNOWLEDGMENTS

This work was supported in part by the NSF (Contract No. EPS-0447679), the DOE (Contracts No. DE-FG02-86ER45271, No. DE-FG02-84DR45170, and No. DE-FG02-01ER45931), and the AFOSR (Contract No. F49620-03-1-01-75).

*Corresponding author. Present address: 5110 Rockhill Road, 257 Flarsheim Hall. FAX: 816-235-5221; carusoan@umkc.edu

[1] A. R. Rocha, V. M. Garcia-Suarez, S. W. Bailey, C. J. Lambert, J. Ferrer, and S. Sanvito, Nature Mater. **4**, 335 (2005).
[2] T. S. Santos, J. S. Lee, P. Migdal, I. C. Lekshmi, B. Satpati, and J. S. Moodera, Phys. Rev. Lett. **98**, 016601 (2007).
[3] J. P. Velev, P. A. Dowben, E. Y. Tsymbal, S. J. Jenkins, and A. N. Caruso, Surf. Sci. Rep. **63**, 400 (2008).
[4] A. J. Epstein, MRS Bull. **28**, 492 (2003).
[5] V. N. Prigodin, N. P. Raju, K. I. Pokhodnya, J. S. Miller, and A. J. Epstein, Adv. Mater. **14**, 1230 (2002).
[6] K. I. Pokhodnya, M. Bonner, J.-H. Her, P. W. Stephens, and J. S. Miller, J. Am. Chem. Soc. **128**, 15592 (2006).
[7] I. Žutić, J. Fabian, and S. Das Sarma, Rev. Mod. Phys. **76**, 323 (2004).
[8] S. Ogale, D. Kundaliya, S. Mehraeen, L.-F. Fu, S. Zhang, A. Lussier, J. Dvorak, N. Browning, Y. Idzerda, and T. Venkatesan, Chem. Mater. **20**, 1344 (2008).
[9] D. Kennedy and C. Norman, Science **309**, 75 (2005).
[10] J. Zhang, J. Ensling, V. Ksenofontov, P. Gütlich, A. J. Epstein, and J. S. Miller, Angew. Chem., Int. Ed. **37**, 657 (1998).
[11] J. M. Manriquez, G. T. Yee, R. S. McLean, A. J. Epstein, and J. S. Miller, Science **252**, 1415 (1991).
[12] D. de Caro, M. Basso-Bert, J. Sakah, H. Casellas, J.-P. Legros, L. Valade, and P. Cassoux, Chem. Mater. **12**, 587 (2000).
[13] K. I. Pokhodnya, A. J. Epstein, and J. S. Miller, Adv. Mater. **12**, 410 (2000).
[14] M. A. Girtu, C. M. Wynn, J. Zhang, J. S. Miller, and A. J. Epstein, Phys. Rev. B **61**, 492 (2000).
[15] C. M. Wynn, M. A. Girtu, J. Zhang, J. S. Miller, and A. J. Epstein, Phys. Rev. B **58**, 8508 (1998).
[16] A. J. Epstein, S. Etemad, A. F. Garito, and A. J. Heeger, Phys. Rev. B **5**, 952 (1972).
[17] P. A. Dowben, J. Phys.: Condens. Matter **19**, 310301 (2007).
[18] N. P. Raju, T. Savrin, V. N. Prigodin, K. I. Pokhodnya, J. S. Miller, and A. J. Epstein, J. Appl. Phys. **93**, 6799 (2003).
[19] C. Tengstedt, M. P. de Jong, A. Kanciurzewska, E. Carlegrim, and M. Fahlman, Phys. Rev. Lett. **96**, 057209 (2006).
[20] C. Tengstedt, M. Unge, M. P. de Jong, S. Stafstrom, W. R. Salaneck, and M. Fahlman, Phys. Rev. B **69**, 165208 (2004).
[21] J. B. Kortright, D. M. Lincoln, R. S. Edelstein, and A. J. Epstein, Phys. Rev. Lett. **100**, 257204 (2008).
[22] P. D. Johnson, Rep. Prog. Phys. **60**, 1217 (1997).
[23] W. Y. Ching, in *The Magnetism of Amorphous Metals and Alloys*, edited by J. A. Fernandez-Baca and W. Y. Ching (World Scientific, Singapore, 1995), p. 85.
[24] R. L. Kurtz and V. E. Henrich, Phys. Rev. B **28**, 6699 (1983).
[25] R. J. Lad and V. E. Henrich, Phys. Rev. B **39**, 13478 (1989).
[26] P. A. Dowben and R. J. Skomski, J. Appl. Phys. **95**, 7453 (2004).
[27] Pramod Bhatt, E. Carlegrim, A. Kanciurzewska, M. P. de Jong, and M. Fahlman, Appl. Phys. A **95**, 131 (2009).
[28] S. J. Luo and K. L. Yao, Phys. Rev. B **67**, 214429 (2003).
[29] M.-H. Wu and W.-D. Zou, J. Math. Chem. **40**, 319 (2006).
[30] R. Arita, Y. Suwa, K. Kuroki, and H. Aoki, Phys. Rev. Lett. **88**, 127202 (2002).
[31] E. Vescovo, H.-J. Kim, Q.-Y. Dong, G. Nintzel, D. Carlson, S. Hulbert, and N. V. Smith, Synchrotron Radiat. News **12**, 10 (1999).